A novel description of FDG excretion in the renal system: application to metformin-treated models

S Garbarino†$, G Caviglia†, G Sambuceti§‡, F Benvenuto* and M Piana†$

† Dipartimento di Matematica, Università di Genova, via Dodecaneso 35, 16146 Genova, Italy
$ CNR - SPIN Genova, via Dodecaneso 33, 16146 Genova, Italy
‡ IRCCS San Martino IST, Largo R Benzi 10, 16132 Genova, Italy
* Ecole Polytechnique, Paris, France
§ Dipartimento di Scienze della Salute, Università di Genova, Largo R Benzi 10, 16132 Genova, Italy

Abstract. This paper introduces a novel compartmental model describing the excretion of 18F-fluoro-deoxyglucose (FDG) in the renal system and a numerical method based on maximum likelihood for its reduction. This approach accounts for variations in FDG concentration due to water re-absorption in renal tubules and for increase of bladder's volume during the FDG excretion process. From the computational viewpoint the reconstruction of the tracer kinetic parameters is obtained by solving the maximum likelihood problem iteratively, using a non-stationary steepest descent approach that explicitly accounts for the Poisson nature of nuclear medicine data. The reliability of the method is validated against two sets of synthetic data realized according to realistic conditions. Finally we applied this model to describe FDG excretion in the case of animal models treated with metformin. In particular we show that our approach allows the quantitative estimate of the reduction of FDG de-phosphorilation induced by metformin.

1. Introduction

Positron Emission Tomography (PET) with 18F-fluoro-deoxyglucose (FDG) has represented a breakthrough in the estimate of cancer metabolic activity and it is successfully used not only for the characterization of cancer infiltration but also for the monitoring of the tissue response to chemo- or radio-therapy. In fact, glucose consumption by malignant cells tends to increase [15], rendering FDG uptake a valuable index of cancer aggressiveness and patient outcome [1]. Nevertheless, clinical activity asks to represent this variable as standardized uptake value (SUV) whose estimation is hampered by the interference of several variables modulating tracer availability independently of tumor metabolism [6]. Among these factors, kidney function plays a relevant role as, differently from the tracked glucose, FDG is scarcely reabsorbed in renal tubule and is largely excreted in the urines [24].

Under physiological conditions, glycosuria is virtually absent in mammalians with serum glucose concentration $< 1.8 - 2\,g/L$, as the metabolite filtered through the glomerular membrane is fully reabsorbed by two dedicated energy-requiring transport systems. These are the Na-Glucose transport carriers (SGLT) that are sequentially expressed on renal tubule with SGLT I being present in its proximal part, and SGLT II in its distal segment. Differently from facilitative transporters (GLUT) expressed in all cells of the body, these two carrier systems display a markedly lower affinity for FDG than for glucose, accounting for the significant urinary tracer loss [18]. This molecular machinery recently gained a renovated interest due to the high antihyperglycemic effect of SGLT II inhibition as an innovative treatment for diabetes mellitus. Besides the therapeutic potential, urinary loss of glucose and of FDG might modify the diagnostic interpretation of PET/CT studies in diabetics patients with cancer. Under this condition, analysis of FDG distribution is often problematic, as the limited uptake of glucose and FDG by insulin dependent tissues is paralleled by the persistence of high tracer concentrations in plasma. Obviously, the ubiquitary presence of radioactive blood smoothens the difference between the pathologic uptake in cancer and the physiological tracer retention in background surrounding tissues. Accordingly, interventions able to increase urinary FDG loss might improve image quality in the large number of diabetic patients submitted to PET/CT for cancer studies. However, testing this hypothesis asks to first verify whether and to what extent a fraction of urinary FDG is indeed reabsorbed by tubule SGLT, implying the availability of methods able to describe the different mechanisms tuning FDG kinetics within the renal compartments.

The standard way to quantitatively determine the efficiency of urinary excretion in nuclear medicine is based on **either measurements of the mean renal clearance or the application of compartmental analysis techniques. Mean renal clearance is defined as the ratio between the asymptotic activity in the bladder and the integral over the whole time interval of the plasma input function [20]. On the other hand, compartmental analysis typically leads to graphical methods [21] and typically involves two compartments: one where the tracer is free and one where the tracer is trapped inside the cells due to 6-phosphorylation.** However, the potential of these conventional approaches is notably hindered by several factors: 1) it is difficult to estimate urinary tracer loss in renal pelvis, due to the fact that the urinary flow is extremely high and can be variable during the experiment; 2) FDG concentration is influenced by fluid and nutrients re-absorption anatomically occurring in the tubule; 3) it is not possible to quantitatively estimate the renal excretion without involving a pool for the tracer anatomically represented by the bladder.

This paper describes the FDG excretion process by taking advantage of microPET studies in mice, using a system that simultaneously covers the whole animal body, allowing the measurement of the tracer amount sequestered over time in the bladder [7]. Further, it introduces a novel compartmental model (see Figure 1) involving:

- An extravascular compartment accounting for tracer outside cells, whose exchange with blood is free.

- **A compartment involving the 6-Phosphorylated FDG, the FDG in cells and the preurine pool accounting for tracer filtered in the preurines and entering the proximal tubule. This compartment contains the majority of tracer in the kidneys. We call this component as metabolized compartment to indicate the fact that in it FDG can also be in the FDG-6P form.**
- The tubular compartment, in which tracer concentration can vary because of water reabsorption.
- The urinary pool representing the ultimate tracer excretion that is measured in the bladder.

There are two main differences between the model in [7] and the one in the present paper and, according to us, both are significant. First, the previous model considered a bladder with constant volume while in this model the bladder volume may vary, as it actually occurs during the physiological process. From a mathematical viewpoint, this update changes the differential equations describing the model and makes such equations more complicated to solve. Second, differently from [7], the model in Figure 1 accounts for the presence of water re-absorption in tubule, with consequent variation of the tracer concentration in the tissue. This update of the model has impact on the tracer kinetic parameters describing the tracer flow from the kidney to the bladder.

As all compartmental models, also this one is mathematically described in terms of a system of Ordinary Differential Equations (ODEs) for concentrations, with appropriate initial conditions. However, in this specific case, the inverse problem of determining the tracer coefficient from nuclear medicine data collected at different time points from ROIs in the reconstructed images is significantly more difficult. Indeed now the number of unknowns is significantly higher while the number of equations is still limited by the limited number of data provided by nuclear medicine. The present paper shows that this inverse problem can be effectively and accurately solved by means of a maximum likelihood approach in which an iterative steepest descent scheme optimizes the Kullbach-Leibler discrepancy [4] between the unknowns and the experimental data. The main advantages of this method with respect to more standard optimization techniques [22] are in the fact that, in the solution process, it explicitly exploits the a priori knowledge represented by the Poisson nature of the measurements, the computational cost is notably reduced and the scheme is very robust with respect to initialization. Specifically, we are able to reduce the computational cost thanks to this robustness, that allows us not to apply a demanding multiple starting technique [3].

We validated the effectiveness of this model first by using synthetic data which have been simulated by mimicking the acquisition process of an actual micro-PET system for small animals. We investigated the reliability of our approach also in the case of

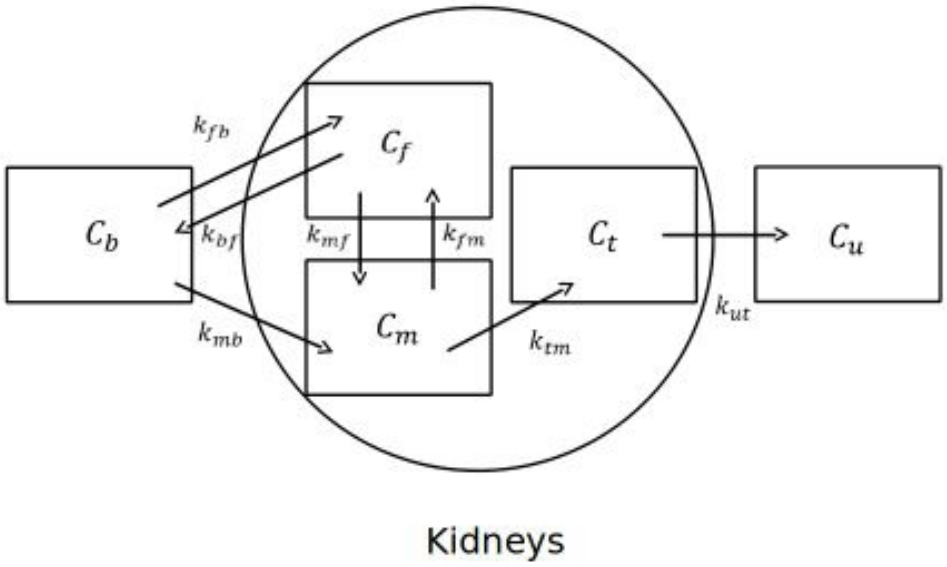

Figure 1. Scheme of the compartmental model used in this paper.

experimental measurements acquired on mice treated with metformin. This drug reduces blood glucose concentration without causing hypoglycemia [14], mostly by decreasing intestinal glucose absorption and glucose delivery by the liver [16]. It follows that nuclear medicine experiments with such kind of animal models are perfect candidates to validate a compartmental model that has been designed in order to follow the FDG kinetics in the renal system in a refined fashion. Specifically, we considered FDG-PET data acquired for 12 healthy, untreated mice and 12 healthy, metformin-treated models. The results of our analysis confirm that the efficiency of FDG de-phosphorylation is notably reduced by metformin and provide a quantitative estimate of such reduction. Further, the average clearance is strongly correlated with one of the tracer coefficient determined by our model, specifically the one related to the rate of glomerular filtration.

The plan of the paper is as follows. Section 2 provides details on the compartmental model. Section 3 describes the computational method for the solution of the inverse problem. Section 4 contains the validation by means of synthetic data and Section 5 discusses the analysis of measurements acquired by a micro-PET device on metformin-treated models. Our conclusions are offered in Section 6.

2. Model for tracer evolution

Standard compartmental analysis [8, 12, 19, 21, 23, 25, 7] models the renal tracer kinetics by means of two functionally (but not spatially) distinct compartments: the tissue in which the tracer is free, $\mathcal{C}_f$, and **the metabolized component** $\mathcal{C}_m$. Since we want to quantitatively assess the role of SGLT-based mechanisms transporting FDG back to metabolism, here we also include the re-absorption compartment $\mathcal{C}_t$, anatomically identified with the tubular system; finally, the urine $\mathcal{C}_u$ represents the pool where the tracer is accumulated and is anatomically identified with the bladder. The tracer concentrations C_f, C_m, C_t and C_u associated to these four compartments are well-defined state variables measured in Bq ml^{-1}. These state variables satisfy the following Cauchy problem, expressing the balance of tracer between compartments:

$$\dot{C}_f = -(k_{bf} + k_{mf})\, C_f + k_{fm}\, C_m + k_{fb}\, C_b, \tag{1}$$

$$\dot{C}_m = k_{mf}\, C_f - (k_{fm} + k_{tm})\, C_m + k_{mb}\, C_b, \tag{2}$$

$$\dot{C}_t = -k_{ut}\, C_t + k_{tm}\, C_m, \tag{3}$$

$$\frac{d}{dt}(V_u\, C_u) = F_{ut}\, C_t, \tag{4}$$

where the superposed dot denotes the time derivative d/dt and the initial conditions are given by

$$C_f(0) = C_m(0) = C_t(0) = C_u(0) = 0. \tag{5}$$

The constants k_{ab} (min^{-1}) represent the exchange coefficients (rate constants or tracer kinetic parameters) between compartments in contact; the suffixes a and b in k_{ab} denote the target and source compartment, respectively. The coefficients are positive and the plus, minus signs characterize incoming and outgoing fluxes, respectively. The peculiarity of equation (4) with respect to the other equations is in the fact that the bladder $\mathcal{C}_u$ is the only compartment whose volume changes in time. In particular, this equation states that the urine accumulates in $\mathcal{C}_u$ at a rate which is constant (because of the resting state of mice), with a bulk flow F_{ut} (ml min^{-1}) entering $\mathcal{C}_u$ from $\mathcal{C}_t$. Finally, C_b, representing the tracer concentration in the blood, is named *Input Function* (IF) and plays the role of trigger for the process of tracer kinetics in the system. This corresponds to considering a Single Input Model, which is more feasible than the Dual Input Model [27, 26] for application of micro-PET analysis to mice.

By combining equations (1)-(4) it is rather straightforward to obtain

$$\begin{aligned} &\dot{C}_f + \dot{C}_m = -k_{bf}\,(C_f + C_m) + \\ &+(\frac{k_{bf}}{k_{tm}} - 1)\,[\frac{1}{F_{ut}}\,\frac{d^2}{dt^2}(V_u\, C_u) + \frac{k_{ut}}{F_{ut}}\,\frac{d}{dt}(V_u\, C_u)] + (k_{fb} + k_{mb})\, C_b \end{aligned} \tag{6}$$

and

$$\frac{d^2}{d^2t}(V_u C_u) = \frac{F_{ut} k_{tm} D}{k_{ut}(k_{bf} - k_{tm})}(C_f + C_m) + \tag{7}$$

$$+\frac{F_{ut}k_{tm}(k_{fm}+k_{tm}+k_{mf})}{k_{ut}(k_{bf}-k_{tm}}(\dot{C}_f+\dot{C}_m)-$$
$$-\frac{1}{k_{ut}}\frac{d^3}{dt^3}(V_uC_u)-\frac{F_{ut}\alpha}{(k_{bf}-k_{tm})k_{ut}}\dot{C}_b,$$

where

$$D=k_{mf}k_{tm}+k_{bf}k_{fm}+k_{bf}k_{tm} \tag{8}$$

and

$$\alpha=(k_{fm}+k_{tm}+k_{mf})k_{fb}+(k_{mf}+k_{bf}+k_{mf})k_{mb}. \tag{9}$$

We now observe that the total radioactivity concentration in the kidneys, C_K, can be written as [13]

$$C_K=\eta_b\,C_b+(1-\eta_b-\eta_t)\,(C_f+C_m)+C_t\,\eta_t, \tag{10}$$

where η_t and η_b are the fractions of kidney volumes V_K occupied, respectively, by the tubular compartment and the blood. Integrating once equation (6) and twice equation (7) in time and using equation (10) lead to

$$A_K=V_K\,\eta_b\,C_b-V_K\,k_{bf}\int_0^t C_K(\tau)d\tau+ \tag{11}$$
$$V_K\,[\eta_b\,k_{bf}+(1-\eta_b-\eta_t)\,(k_{fb}+k_{mb})]\int_0^t C_b(\tau)d\tau+$$
$$+V_K\left(k_{bf}\,\frac{\eta_t}{F_{ut}}+\beta\,k_{ut}\right)V_u\,C_u+V_K\left(\frac{\eta_t}{F_{ut}}+\beta\right)\frac{d}{dt}(V_u\,C_u)$$

and

$$A_u=\frac{1}{\gamma}[\frac{F_{ut}k_{tm}k_{mf}}{1-\eta_b-\eta_t}\int_0^t d\tau\int_0^\tau d\tau' C_K(\tau')+ \tag{12}$$
$$(F_{ut}k_{tm}k_{mb}-\frac{F_{ut}k_{tm}k_{mf}}{1-\eta_b-\eta_t}\eta_b)\int_0^t d\tau\int_0^\tau d\tau' C_b(\tau')-$$
$$-\frac{d}{dt}(V_uC_u)-(\frac{k_{tm}k_{mf}\eta_t}{1-\eta_b-\eta_t}+(k_{fm}+k_{tm}+k_{mf})k_{ut})\int_0^t(V_uC_u)(\tau)d\tau],$$

where

$$A_K=V_K\,C_K, \tag{13}$$

$$\beta=\frac{1-\eta_b-\eta_t}{F_{ut}}\,(\frac{k_{bf}}{k_{tm}}-1), \tag{14}$$

$$A_u=V_u\,C_u. \tag{15}$$

and

$$\gamma:=k_{ut}+k_{fm}+k_{tm}+k_{mf}. \tag{16}$$

A_K and A_u denote the total radiactivity in kidneys and bladder, respectively. Both equation (11) and equation (12) can be simplified by observing that the terms containing $d/dt(C_uV_u)$ are much smaller than the terms in the sums at the right hand

sides (this behavior can be easily observed by numerical computation). Therefore the (approximated) *global balance equations* for the tracer in this compartmental model are

$$A_K = x_1\, V_K\, C_b + x_2 \int_0^t A_K + x_3\, V_K \int_0^t C_b + x_4 V_K\, V_u\, C_u, \tag{17}$$

and

$$A_u = z_1 \int_0^t \int_0^\tau C_K + z_2 \int_0^t \int_0^\tau C_b + z_3 \int_0^t V_u\, C_u, \tag{18}$$

where the column vectors of macroparameters, x and z, are defined by the equations

$$\begin{aligned} &(x_1, x_2, x_3, x_4)^T := \\ &\Big(\eta_b,\quad -k_{bf},\quad \eta_b\, k_{bf} + (1-\eta_b-\eta_t)\,(k_{fb}+k_{mb}),\quad k_{bf}\,\frac{\eta_t}{F_{ut}} + \beta\, k_{ut}\Big)^T, \end{aligned} \tag{19}$$

and

$$\begin{aligned} &(z_1, z_2, z_3)^T := \\ &\frac{1}{\gamma}\Big(\frac{F_{ut}k_{tm}k_{mf}}{1-\eta_b-\eta_t}, F_{ut}k_{tm}k_{mb} - \frac{F_{ut}k_{tm}k_{mf}}{1-\eta_b-\eta_t}, -\frac{k_{tm}k_{mf}\eta_t}{1-\eta_b-\eta_t} - (k_{fm}+k_{tm}+k_{mf})k_{ut}\Big)^T \end{aligned} \tag{20}$$

with T denoting the matrix transpose.

In equations (17) and (18) the activities A_K and A_u represent the input experimental data. They are obtained by drawing Region of Interests (ROIs) on PET images at different time points, in correspondence with kidneys and bladder, respectively. The Input Function (IF) C_b is obtained in an analogous way, using ROIs on the left ventricle. On the other hand, the equation solutions x and z contain the physiological unknowns of the process, i.e. the tracer kinetic parameters $k_{bf}, k_{mf}, k_{fm}, k_{fb}, k_{tm}, k_{mb}, k_{ut}$, together with the volume fractions η_b and η_t and the flux F_{ut}. However, before considering the numerical solution of the two equations, we introduce two physiological constraints that reduce the number of these unknowns. First, we observe that, according to the assumption of stationarity, the constant flux rate of the fluid into bladder F_{ut} can be estimated from the measured bladder volumes $V_u(t_f)$, at the final time t_f, and $V_u(\bar{t})$, at an intermediate time $\bar{t}$ as

$$F_{ut} = \frac{V_u(t_f) - V_u(\bar{t})}{t_f - \bar{t}}. \tag{21}$$

It follows that F_{ut} is given by the experimental knowledge of V_u at different time points. Second, we have to account for the outgoing flux rate of free fluid from the compartment $\mathcal{C}_t$. Table 1 in [17] shows that the bulk flow of carrier fluid toward the bladder is around two orders of magnitude smaller than the re-absorbed flow. **Since the volume of the re-absorption compartment is a measurable anatomical volume, the tracer balance equation in tubule implies $k_{tm} = 10^2 k_{ut}$.** Moreover it follows from the definitions that $k_{ut}\eta_t V_K = F_{ut}$.

3. Optimization algorithm

PET activities are acquired at different time points $t_1, \ldots, t_N$ according to pre-defined acquisition paradigms. This implies the following discretization of equations (17) and (18):

$$y_i = A_K(t_i), \qquad w_i = A_u(t_i), \qquad i = 1, 2, \ldots, N, \tag{22}$$

where y and w are N-dimensional column vectors; A is the $N \times 4$ matrix with rows

$$V_K\, C_b(t_i), \quad \int_0^{t_i} A_K\; d\tau, \quad V_K \int_0^{t_i} C_b\; d\tau, \quad V_R\, V_u\, C_u(t_i) \tag{23}$$

$i = 1, 2, \ldots N$; B is the $N \times 3$ matrix with rows

$$\int_0^{t_i} \int_0^{\tau} C_K\; d\tau\; d\tau', \quad \int_0^{t_i} \int_0^{\tau} C_b\; d\tau\; d\tau', \quad \int_0^{t_i} V_u C_u\; d\tau, \tag{24}$$

$i = 1, 2, \ldots N$ (according to definitions (23) and (24) the elements of $\mathbf{A}$ and $\mathbf{B}$ are positive). Therefore the discretized versions of equations (17) and (18) for x and z take the forms

$$y = \mathbf{A}x \tag{25}$$

and

$$w = \mathbf{B}z. \tag{26}$$

Optimization methods are systematically applied in compartmental analysis with the aim of numerically determining the tracer kinetic parameters [8, 12, 19, 21, 9, 23]. However, the optimization problem defined by equations (25) and (26) is characterized by two peculiarities that make it significantly different with respect to more traditional frameworks. First, most compartmental models of the renal system include just two functional compartments, both anatomically embedded (but not anatomically distinguishable) in the kidneys. On the contrary here we have a third (functional and anatomical) compartment represented by the tubular structures and describing the increase of tracer concentration resulting from the re-absorption process of water by tubules; and a fourth anatomical compartment, the bladder, which simply accumulates the excreted tracer during the output process. This implies that the number of unknowns in the present case is much higher and that traditional optimization schemes may not work properly for this model. The second peculiarity of equations (25) and (26) is that, in both cases, the data are activities, while in standard compartmental analysis the data are concentrations. This has an important technical implication since activities are affected by Poisson noise and this piece of a priori information can be exploited in the parameter identification process by applying a maximum likelihood approach in which the likelihood is provided by the Poisson-statistics-inspired Kullbach-Leibler divergence. In the following we define this approach to optimization in the case of equation (25). The extension to equation (26) is straightforward.

Maximum likelihood is a standard statistical approach for estimating the vector parameter x given y, which is based on the assumption that the given vector y is an

observed value of the random vector Y with mean $\mathbf{A}x$. Denoting by η the corresponding random process (a Poisson process, in the present case), we have

$$Y_i = \eta_i(\mathbf{A}x) \tag{27}$$

$i = 1, \ldots, N$. The density function of the vector Y is given by the joint probability density function $p_\eta(y, \mathbf{A}x)$. When this density is thought of as a function of x given y, we refer to it as the likelihood, and we write

$$\mathcal{L}_y(x) = p_\eta(y, \mathbf{A}x). \tag{28}$$

Once the matrix $\mathbf{A}$ and the datum y are given, maximum likelihood finds the solution of x when the likelihood reaches its maximum values. The maximum likelihood estimator is then

$$\tilde{x} = \arg\max_{x \in \mathbf{R}^4} \mathcal{L}_y(x). \tag{29}$$

Usually it is more convenient to minimize the negative logarithm of the likelihood instead of maximizing it. The maximum likelihood problem is then equivalent to

$$\tilde{x} = \arg\min_{x \in \mathbf{R}^4} L_y(x), \tag{30}$$

where $L_y(x) = -\log(\mathcal{L}_y(x))$. In our case η is a vector of indipendent and identically distributed Poisson variables with parameter given by $\mathbf{A}x$, so that the negative logarithm of the likelihood is equivalent to the Kullback Leibler divergence [4]

$$D_{KL}(y, x) = \frac{2}{N} \sum_{i=1}^{N} y_i \log \frac{y_i}{(\mathbf{A}x)_i} + (\mathbf{A}x)_i - y_i + y_i \log(y_i). \tag{31}$$

Hence (29) is equivalent to the minimization of $D_{KL}(x, y)$. We are interested in building up an iterative algorithm that can reach the minimum of D_{KL} in a finite number of iterations. When the positivity constraint on the solution applies, this can be done by means of expectation maximization approaches, according to a fixed point successive approximation scheme. Since here the components of x are not all positive, we use a non-stationary steepest descent method such that

$$x^{(k+1)} = x^{(k)} - \tau^{(k)} \nabla D_{KL}(y, x), \tag{32}$$

where $\tau^{(k)}$ is the step size which is allowed to change at each iteration. We choose τ such that:

(i) $\tau^{(k)} > 0$ for all k;

(ii) $(\mathbf{A}x^{(k+1)})_i > 0$ for every iteration k and for every $i = 1, \ldots, N$;

(iii) $D_{KL}(y, x^{(k+1)}) \leq D_{KL}(y, x^{(k)})$ for every iteration k.

With this choice, we can effectively build up a D_{KL}-decreasing algorithm (thanks to (i) and (iii)) and we are guaranteed that the logarithm that appears in the computation of D_{KL} makes sense (thanks to (ii)). Therefore the algorithm we implemented for the solution of equation (25) reads as follows: given $x^{(k)}$,

Step 1: choose $\tau^{(k)}$ such that (ii) holds.

Step 2: compute $x^{(k+1)}$ in (32);

Step 3: if $D_{KL}(y, x^{(k+1)}) \leq D_{KL}(y, x^{(k)})$ go on with the iterations. Otherwise

Step 4: decrease $\tau^{(k)}$ until $D_{KL}(y, x^{(k+1)}) \leq D_{KL}(y, x^{(k)})$ and when this happens, go on with the iterations.

The scheme is stopped when $|D_{KL}(x^{(k+1)}) - D_{KL}(x^{(x)})| \cdot |x^{(k+1)} - x^{(k)}| < \epsilon$, with ϵ an appropriate threshold.

4. Numerical validation

An "Albira" micro-PET system produced by Carestream Health is currently operational at the IRCCS San Martino IST, Genova. Experiments with mice are currently performed at this site, by using different tracers, mainly for applications to oncology and to FDG physiology in the renal and liver systems [16, 7]. In this section we describe the performance of our approach to compartmental analysis in the case of synthetic data simulated by mimicking "Albira" acquisitions for FDG-PET experiments.

In order to produce the synthetic data we initially chose realistic values for V_K, $V_u(t_1)$ and F_{ut}; then we utilized six ground truth values for the tracer kinetic parameters k_{bf}, k_{mf}, k_{fm}, k_{fb}, k_{mb} and k_{ut} and for η_b. We also exploited the two relations $k_{tm} = 10^2\, k_{ut}$ and (21). With these selected values we can solve equations (1) and (2) in terms of C_m and C_f; then we solve (3) in term of C_t and finally we can solve (4) and find $V_u C_u$. These solutions of the Cauchy problem are sampled in time, on a total time interval $[t_1, t_N]$ that corresponds to the total acquisition time with "Albira" and in correspondence of time points typical of experiments with "Albira" in this application context. IF C_b has been obtained by fitting with a gamma variate function a set of real measurements acquired from a healthy mouse in a very controlled experiment. Then, using vectors corresponding to the discretization of C_m, C_f, C_t and C_u, it is possible to compute the matrices $\mathbf{A}$ and $\mathbf{B}$, and the data vectors y and w in the same equations (25) and (26). Finally we affected the data by Poisson noise and applied our algorithm in order to reconstruct the exchange coefficients and η_b. We point out that this kind of test is specific for the validation of the physiological model, since the synthetic data have been computed by integrating equations different than the model ones (i.e., no inverse crime has been performed).

We realized two different simulation experiments, with two different but reliable sets of values for the tracer kinetic parameters. For both experiments we set $V_K = 0.15$ ml, $F_{ut} = 0.004$ ml/min and $V_u(t_1) = 0.16$ ml; the two sets for the tracer kinetic parameters are represented in the ground truth (g.t.) row in Table 1 and in Table 2. The signal-to-noise ratios adopted for these tests are 12.4 dB for (25) and 26.3 dB for (26) in the case of the first experiment and 13.6 dB and 27.7 dB for the same equations, in the second experiment. Comparison with the ground truth values for this parameters provides limits about the reliability of the model and of the inversion procedure. Our approach reconstructs the input tracer kinetic parameters with relative errors never

	k_{bf}	k_{ut}	k_{mf}	k_{fb}	k_{fm}	k_{mb}	η_b
g. t.	0.60	1.30	0.60	1.00	0.20	0.30	0.20
our method	0.63 ± 0.04	1.31 ± 0.05	0.60 ± 0.01	1.01 ± 0.03	0.21 ± 0.02	0.32 ± 0.03	0.22 ± 0.04
LS	0.67 ± 0.16	1.34 ± 0.31	0.66 ± 0.12	1.12 ± 0.19	0.26 ± 0.10	0.32 ± 0.11	0.19 ± 0.09

Table 1. Ground truth (g.t.) and reconstructed values for tracer kinetic parameters and η_b for the first simulated experiment, **with both our method and a standard least-squares approach (LS)**. Here $V_K = 0.15$ ml, $F_{ut} = 0.04$ ml min^{-1}, $V_u(t_1) = 0.16$ ml. The signal-to-noise ratios for the activities A_K and A_u are 12.4dB and 26.3dB, respectively.

	k_{bf}	k_{ut}	k_{mf}	k_{fb}	k_{fm}	k_{mb}	η_b
g. t.	0.40	1.00	0.70	0.90	0.02	0.10	0.15
our method	0.41 ± 0.03	1.02 ± 0.04	0.73 ± 0.03	0.92 ± 0.03	0.02 ± 0.01	0.09 ± 0.01	0.16 ± 0.02
LS	0.46 ± 0.19	1.09 ± 0.20	0.72 ± 0.12	0.89 ± 0.11	0.02 ± 0.02	0.11 ± 0.06	0.17 ± 0.06

Table 2. Ground truth (g.t.) and reconstructed values for tracer kinetic parameters and η_b for the second simulated experiment, **with both our method and a standard least-squares approach (LS)**. Here $V_K = 0.15$ ml, $F_{ut} = 0.04$ ml min^{-1}, $V_u(t_1) = 0.16$ ml. The signal-to-noise ratios for the activities A_K and A_u are 13.6dB and 27.7dB, respectively.

larger than 10%. Further, the standard deviations are systematically small, thus showing the notable numerical stability of the iterative reconstruction scheme with respect to noise (mean and standard deviations are computed over 50 runs of the same problem with different (random) initialization vectors $x^{(0)}$ and $z^{(0)}$). **For both the experiments we also applied to the data a standard multilinear fitting approach [2, 5, 11] that assumes Gaussian noise on data and utilizes the Levenberg-Marquardt technique for least-squares minimization. Table 1 and Table 2 show that our approach produces significantly smaller uncertainties (with the same computational burden).**

5. Metformin effects on glucose renal metabolism

We applied the novel compartmental approach introduced in this paper to the investigation of the effects that metformin produces on the glucose excretion process. For our experiment we have considered a control group (n=12) and a group (of the same size) in which FDG injection was performed after one month of high dose metformin treatment (750 mg/Kg body weight daily). In all animals 3700 KBq of FDG were injected into a tail vein after a fasting period of six hours during a dynamic list mode acquisition (10×15s + 1×22s + 4×30s + 5×60s + 2×150s + 5×300s). The images have been reconstructed by applying an Ordered Subset Expectation Maximization (OSEM) iterative algorithm [10] while ROIs have been drawn over kidneys and bladder in order to measure the activities A_K and A_u (see Figure 2). ROIs have been also drawn over the left ventricle in order to compute the IF. **We are aware that the determination**

	k_{bf}	k_{ut}	k_{mf}	k_{fb}	k_{fm}	k_{mb}	η_b	η_t
m1	0.32 ± 0.06	0.30 ± 0.04	0.20 ± 0.05	$(6.21 \pm 0.23)10^{-4}$	$(1.61 \pm 0.41)10^{-3}$	0.08 ± 0.01	0.19 ± 0.02	0.03 ± 0.01
m2	1.29 ± 0.12	1.09 ± 0.08	0.36 ± 0.06	$(9.96 \pm 0.34)10^{-4}$	0.52 ± 0.04	1.32 ± 0.07	0.24 ± 0.02	0.03 ± 0.01
m3	0.21 ± 0.06	0.22 ± 0.04	0.16 ± 0.03	$(6.91 \pm 0.23)10^{-4}$	$(2.59 \pm 0.13)10^{-4}$	0.46 ± 0.09	0.19 ± 0.02	0.09 ± 0.02
m4	0.23 ± 0.07	0.26 ± 0.09	0.02 ± 0.01	$(5.01 \pm 3.14)10^{-4}$	0.05 ± 0.01	1.32 ± 0.09	0.16 ± 0.04	0.04 ± 0.01
m5	0.11 ± 0.02	0.10 ± 0.02	0.10 ± 0.03	$(7.71 \pm 0.35)10^{-3}$	$(9.11 \pm 4.32)10^{-4}$	0.37 ± 0.06	0.14 ± 0.03	0.02 ± 0.01
m6	0.58 ± 0.07	0.56 ± 0.05	0.02 ± 0.01	0.03 ± 0.01	0.02 ± 0.01	0.80 ± 0.09	0.28 ± 0.08	0.03 ± 0.01
m7	0.40 ± 0.06	0.47 ± 0.11	0.13 ± 0.02	$(9.60 \pm 3.02)10^{-3}$	0.23 ± 0.07	1.00 ± 0.14	0.24 ± 0.06	0.05 ± 0.02
m8	0.43 ± 0.05	0.35 ± 0.05	0.20 ± 0.03	$(6.44 \pm 2.01)10^{-4}$	0.10 ± 0.01	1.88 ± 0.10	0.21 ± 0.03	0.03 ± 0.01
m9	0.50 ± 0.06	0.61 ± 0.07	0.11 ± 0.02	$(4.39 \pm 2.72)10^{-4}$	0.09 ± 0.02	0.81 ± 0.06	0.26 ± 0.03	0.04 ± 0.01
m10	0.31 ± 0.05	0.41 ± 0.04	0.18 ± 0.03	$(7.01 \pm 3.32)10^{-4}$	0.06 ± 0.01	0.08 ± 0.01	0.31 ± 0.03	0.05 ± 0.02
m11	0.28 ± 0.02	0.29 ± 0.03	0.21 ± 0.02	$(3.87 \pm 1.57)10^{-4}$	0.04 ± 0.01	0.43 ± 0.03	0.22 ± 0.01	0.03 ± 0.01
m12	0.38 ± 0.06	0.30 ± 0.04	0.12 ± 0.01	$(5.04 \pm 2.09)10^{-4}$	0.24 ± 0.03	0.66 ± 0.05	0.27 ± 0.02	0.04 ± 0.01

Table 3. Tracer kinetic parameters and volume rates for 12 healthy untreated mice representing the control group. **The uncertainties are computed as standard deviations over** 50 **runs of the algorithm with** 50 **different random initialization values.**

	k_{bf}	k_{ut}	k_{mf}	k_{fb}	k_{fm}	k_{mb}	η_b	η_t
m13	0.62 ± 0.08	0.34 ± 0.05	0.04 ± 0.01	0.04 ± 0.02	$(8.59 \pm 1.56)10^{-4}$	0.41 ± 0.04	0.23 ± 0.02	0.02 ± 0.01
m14	0.12 ± 0.02	0.14 ± 0.01	0.02 ± 0.01	0.12 ± 0.02	$(3.65 \pm 0.23)10^{-4}$	0.65 ± 0.10	0.17 ± 0.01	0.01 ± 0.01
m15	1.90 ± 0.12	0.24 ± 0.01	0.08 ± 0.02	0.42 ± 0.09	0.03 ± 0.01	1.84 ± 0.16	0.30 ± 0.05	0.01 ± 0.01
m16	0.51 ± 0.09	0.52 ± 0.11	0.15 ± 0.04	0.20 ± 0.02	0.01 ± 0.01	0.90 ± 0.10	0.27 ± 0.07	0.06 ± 0.02
m17	0.20 ± 0.05	0.11 ± 0.02	0.01 ± 0.01	0.11 ± 0.02	$(1.57 \pm 0.24)10^{-5}$	0.42 ± 0.07	0.31 ± 0.04	0.02 ± 0.01
m18	0.11 ± 0.02	0.17 ± 0.01	0.04 ± 0.01	0.15 ± 0.04	0.01 ± 0.01	0.70 ± 0.13	0.25 ± 0.09	0.07 ± 0.02
m19	0.73 ± 0.13	0.72 ± 0.09	0.10 ± 0.02	0.22 ± 0.05	0.02 ± 0.01	0.06 ± 0.01	0.21 ± 0.07	0.04 ± 0.01
m20	0.38 ± 0.08	0.36 ± 0.04	0.06 ± 0.01	0.01 ± 0.01	$(1.64 \pm 0.48)10^{-4}$	0.91 ± 0.17	0.31 ± 0.07	0.08 ± 0.02
m21	0.49 ± 0.12	0.39 ± 0.05	0.13 ± 0.02	0.01 ± 0.01	$(1.71 \pm 0.09)10^{-3}$	1.23 ± 0.20	0.22 ± 0.07	0.09 ± 0.03
m22	0.36 ± 0.08	0.40 ± 0.10	0.05 ± 0.01	0.02 ± 0.01	$(3.76 \pm 0.21)10^{-4}$	0.42 ± 0.12	0.19 ± 0.02	0.08 ± 0.03
m23	0.39 ± 0.10	0.44 ± 0.11	0.21 ± 0.05	0.11 ± 0.02	$(3.97 \pm 0.21)10^{-4}$	1.85 ± 0.20	0.30 ± 0.03	0.11 ± 0.01
m24	0.13 ± 0.03	0.12 ± 0.01	0.11 ± 0.02	0.01 ± 0.01	$(5.62 \pm 0.31)10^{-4}$	0.06 ± 0.01	0.23 ± 0.03	0.06 ± 0.01

Table 4. Tracer kinetic parameters and volume rates for 12 mice treated with metformin. **The uncertainties are computed as standard deviations over** 50 **runs of the algorithm with** 50 **different random initialization values.**

of IF is a challenging task in the case of mice. To accomplish it, for each animal model we have first viewed the tracer first pass in cine mode. Then, in a frame where the left ventricle was particularly visible, we have drawn a ROI in the aortic arc and maintained it for all time points.

Table 3 and Table 4 contain the reconstructed values of the tracer kinetic parameters for the 12 untreated mice and the 12 metformin-treated mice. Means and standard deviations are computed by using 50 runs of the code for 50 different initializations $x^{(0)}$ and $z^{(0)}$ **(the initialization is performed component-wise for these two vectors, by picking up numbers in the interval** $[0, 1]$ **with uniform distribution)**. Figure 3 contains the average and the standard deviations of the values of the tracer kinetic parameters computed over the treated and untreated mice. This plot shows that k_{fm} decreases of around one order of magnitude when the mice are treated with metformin while the variations of the other tracer kinetic parameters are statistically negligible. Figure 4 studies the correlation between the urinary clearance (ml mm^{-1}) and one of the tracer kinetic parameters, k_{mb}, which indicates the efficiency with which the tracer from blood reaches the preurine compartment. This correlation coefficient is very high in all cases, i.e. by considering separately non-treated and treated mice and by looking at all animals as a unique model set.

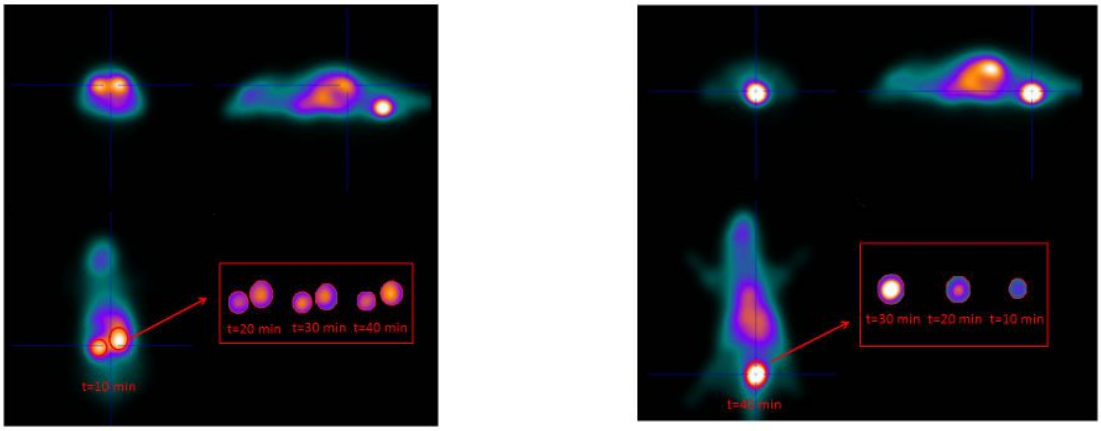

Figure 2. Examples of ROIs on kidneys and bladder at different time points. Left panel: ROIs on kidneys. Right panel: ROIs on bladder.

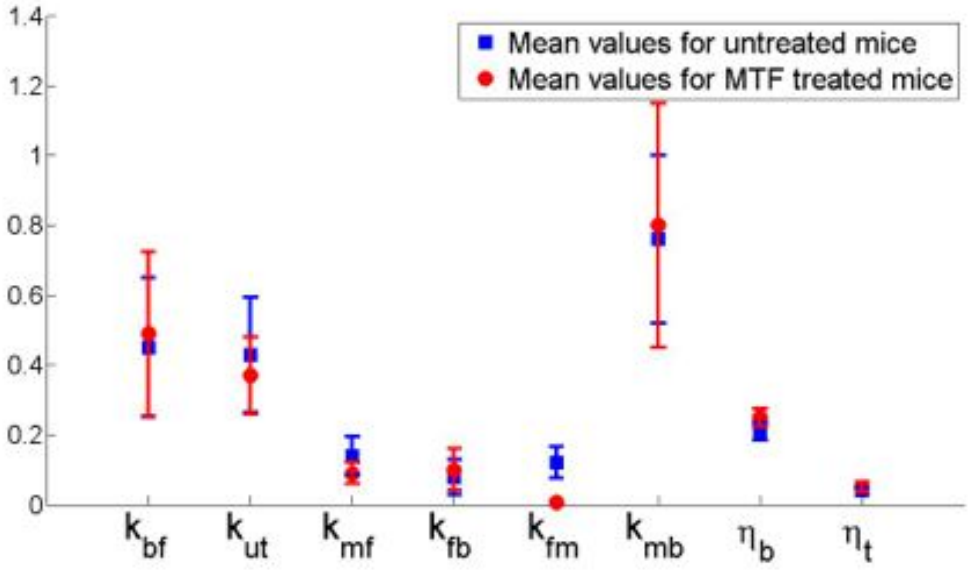

Figure 3. Means and standard deviations for the coefficients reconstructed via the maximum likelihood approach (k_{bf},k_{ut},k_{mf},k_{fb},k_{fm},k_{mb}, η_b and η_t) over the 2 sets of mice. In blue the control group of the healthy untreated mice, in red the group of metformin treated mice. It is possible to notice that k_{fm} is significantly reduced in metformin treated mice.

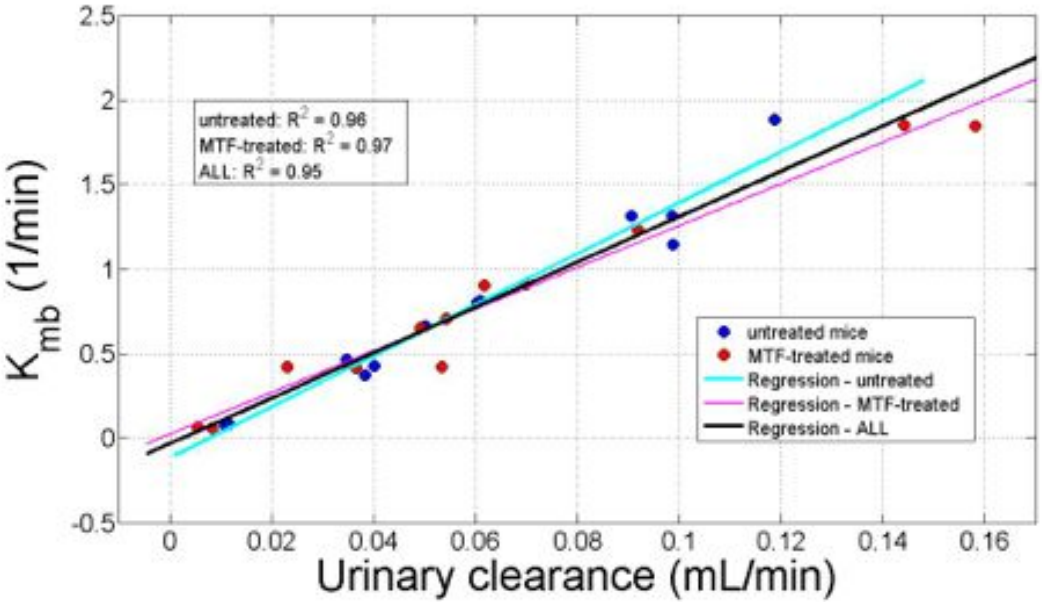

Figure 4. Correlation between the average clearence and the rate coefficients over the control group of 12 healthy untreated mice (light blue line); over the set of the 12 metformin treated mice (magenta line); over the whole set of mice (black line).

6. Comments

This paper introduces a novel description of FDG metabolism in the renal system based on a very general compartmental model. Such model accounts for tracer exchange within and outside cells, the amount of tracer filtered in the preurines and entering the proximal tubule, the variation of tracer concentration due to water reabsorption and tracer accumulation in the bladder. From a computational viewpoint, this model relies on a maximum likelihood approach that explicitly accounts for the Poisson nature of the data statistics and in which the optimization is obtained iteratively, by means of a steepest descent scheme.

From the physiological viewpoint, the description of the renal FDG handling provided by our compartmental analysis is pictured in Figure 5 where the black arrows indicate all the tracer kinetic parameters computed by the method and changes in the thickness of such arrows indicate variations of the coefficient values. **Figure 4 shows that there exists a strong correlation between k_{mb} and the mean urinary clearance, and so that glomerular filtration (expressed in our compartmental framework just by k_{mb}) is the major determinant of possible tracer elimination in the urines [18]. Further, our model allows one to assess the reabsorption process in tubule independently from renal clearance. More importantly, the transfer constant k_{fm} (describing the path from cells and pre-urine back to the interstitial space) is the only parameter influenced by metformin. Indeed, Figure 3 shows that k_{fm} significantly decreases**

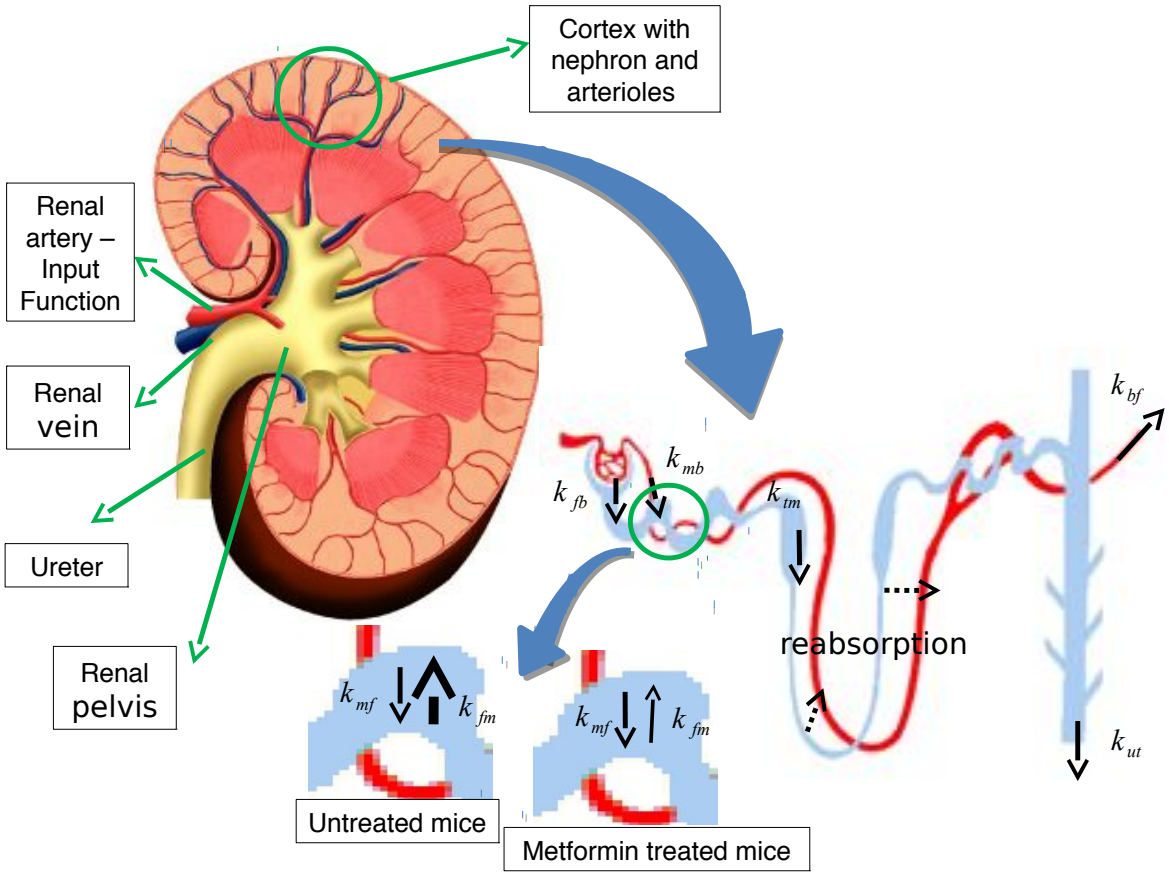

Figure 5. Picture of the FDG excretion process as designed by the novel compartmental model. Arterioles are represented in red and tubules in light blue. The black arrows correspond to the computed tracer kinetic parameters. The thickness variation in the arrows corresponds to the variation of the coefficient values as reconstructed by the maximum likelihood approach.

in metformin-treated mice with respect to untreated animals (this is in agreement with the metformin property to modify the molecular pathways active on this process [16]). Finally, Figure 5 provides a global picture of the kinetic parameters determined via our model and, in particular thickness variation in arrows corresponds to variation in the parameters values.

From a methodological viewpoint, our computational approach might represent a new tool to facilitate the analysis of FDG kinetic response to drug interventions aimed to increase tracer clearance in those patients where the prolonged FDG persistence in blood can deteriorate the accuracy of PET /CT evaluation of tumor metabolism. This problem is particularly frequent in diabetic patients, for whom hyperglycemia is often associated to an impaired renal function and reduced glomerular filtration rates. In these patients, inhibition of tubule reabsorption mechanism and the consequent acceleration in blood tracer clearance might represent a possible way to improve image quality.

References

[1] Adams S, Baum R P, Stuckensen T, Bitter K and Hoer G 1998 Prospective comparison of FDG-PET with conventional imaging modalities (CT, MRI, US) in lymph node staging of head and neck cancer *Eur. J. Nucl. Med.* **25** 1255-1260

[2] Alpert N M, Badgaiyan R D, Livni E and Fischman A J A novel method for noninvasive detection of neuromodulatory changes in specific naurotransmitter system *Neuroimage* **19** 1049-1060

[3] Ahearn T, Staff R, Redpath T and Semple S 2005 The use of Levenberg Marquardt curve fitting algorithm in pharmacokinetic modelling of DCE MRI data *Phys. Med. Biol.* **50** 85-72

[4] Cover T M and Thomas J A 1991 *Elements of information theory* (Wiley, New York)

[5] Blomqvist G 1984 On the Construction of Functional Maps in Positron Emission Tomography *J. Cereb. Flow Metab.* **4** 629-632

[6] Diederichs C G, Staib L, Glatting G, Beger H G and Reske S N 1998 FDG PET: Elevated plasma glucose reduces both uptake and detection rate of pancreatic malignancies *J. Nucl. Med.* **39** 1030-1033

[7] Garbarino S, Caviglia G, Brignone M, Massollo M, Sambuceti G and Piana M 2013 Estimate of FDG excretion by means of compartmental analysis and Ant Colony Optimization *Comput. Math. Methods Med.* **2013** 793142 10 pages

[8] Gunn R N Gunn S R and Cunningham V J 2001 Positron Emission Tomography Compartmental *Models J. Cereb. Flow Metab.* **21** 635-652

[9] Gunn R N, Gunn S R, Turkheimer F E, Aston J A D and Cunningham V J 2002 Positron Emission Tomography Compartmental Models: a basis pursuit strategy for Kinetic Modeling, *J. Cereb. Flow Metab.* **22** 1425-1439

[10] Hudson H M and Larkin R S 1994 Accelerated image reconstruction using ordered subsets of projection data *IEEE Trans. Med. Imag.* **13** 601-609

[11] Ichise M, Liow J S, Lu J Q, Takano A, Model K, Toyama H, Suhara T, Suzuki K, Innis R B and Carson R E 2003 Linearized Reference Tissue Parametric Imaging Methods: Application to [11C]DASB Positron Emission Tomography Studies of the Serotonin Transporter in Human Brain *J. Cereb. Flow Metab.* **23** 1096-1112

[12] Kamasak M E, Bouman C A, Morris E D and Sauer K 2005 Direct Reconstruction of Kinetic Parameter Images From Dynamic PET Data *IEEE Trans. Med. Imag.* **24** 636-650

[13] Kimura Y, Naganawa M, Shidahara M, Ikoma Y and Watabe H 2007 PET kinetic analysis - Pitfalls and a solution for the Logan plot *Ann. Nucl. Med.* **21** 1-8

[14] Klepser T B and Kelly M W 1997 Metformin hydrochloride: an antihyperglycemic agent *Am. J. Health-System Pharm.* **54** 893-903

[15] Lindholm P, Minn H, Leskinen-Kallis S, Bergman J, Ruotsalainen U and Joenssen H 1993 Influence of the blood glucose concentration on FDG uptake in cancer - a PET study *J. Nucl. Med.* **34** 1-6

[16] Massollo M, Marini C, Brignone M, Emionite L, Salani B, Riondato M, Capitanio S, Fiz F, Democrito A, Amaro A, Morbelli S, Piana M, Maggi D, Cilli M, Pfeffer U and Sambuceti G 2013 Metformin temporal and localized effects on gut glucose metabolism assessed using 18F-FDG PET in mice *J. Nucl. Med.* **54** 259-266

[17] Meneton P, Ichikawa I, Inagami T and Schnermann J 2000 Renal physiology of the mouse *Am. J. Phys. - Renal Phys.* **278** F339-F351

[18] Moran J K, Lee H B and Blauford M D 1999 Optimization of urinary FDG excretion during PET imaging *J. Nucl. Med.* **40** 1352-1357

[19] Qiao H, Bai J, Chen Y and Tian J 2007 Kidney modelling for FDG excretion with PET *Int. J. Biomed. Imag.* **2007** 63234 4 pages

[20] Rescigno A 1997 Clearance, turnover time, and volume of distribution *Pharm. Res.* **35** 189-193

[21] Schmidt K C and Turkheimer F E 2002 Kinetic modeling in positron emission tomography *Q. J. Nucl. Med. Mol. Imag.* **46** 70-85

[22] Schwefel 1995 *Evolution and optimum seeking* (Wiley, New York)

[23] Shen Y, Liu H, Shi P 2010 Limited view PET reconstruction of tissue radioactivity maps *Comput. Med. Imag. Grap.* **34** 142-148

[24] Shreve P D, Anzai Y and Wahl R L 1999 Pitfalls in oncologic diagnosis with FDG PET imaging: physiological and benign variants *RadioGraphics* **19** 61-77

[25] Sourbron S and Buckley D 2012 Tracer kinetic modelling in MRI: estimating perfusion and capillary permeability *Phys. Med. Biol* **57** R1-R33

[26] Tichauer K, Samkoe K, Klubben W, Hasan T and Pogue B 2012 Advantages of a Dual-Tracer model over Reference Tissue models for Binding Potential measurement in tumors *Phys. Med. Biol.* **57** 6647-6659

[27] Tomasi G, Kimberley S, Rosso L, Aboagye E and Turkheimer F 2012 Double-Input compartmental modelling and spectral analysis for the quantification of Positron Emission Tomography data in oncology *Phys. Med. Biol.* **57** 1889-1906